Center of mass scaling in three-dimensional binary granular systems

C. R. K. Windows-Yule and D. J. Parker
School of Physics and Astronomy, University of Birmingham, Edgbaston, Birmingham B15 2TT, United Kingdom
(Received 2 April 2014; revised manuscript received 17 May 2014; published 24 June 2014)

Using a combination of experimental results acquired through positron emission particle tracking and simulational results obtained via the discrete particle method, we determine a scaling relationship for the center of mass height of a vibrofluidized three-dimensional, bidisperse granular system. We find the scaling to be dependent on the characteristic velocity with which the system is driven, the depth of the granular bed, and the elasticities of the particles involved, as well as the degree of segregation exhibited by the system and the ratio of masses between particle species. The scaling is observed to be robust over a significant range of system parameters.

DOI: 10.1103/PhysRevE.89.062206 PACS number(s): 81.05.Rm, 45.70.Mg

I. INTRODUCTION

Vibrated granular materials are known to exhibit a plethora of interesting phenomena, including behaviors analogous to those observed in classical fluids, such as convection [1,2] and surface patterns [3] as well as those without parallel in molecular materials, such as the tendency of granular mixtures to spontaneously separate [4,5]. Although there exists a significant body of work concerning vibrated granular systems, and despite their relevance to many diverse industrial applications [6–10], much of their behavior remains poorly understood. One manner in which researchers attempt to address this issue is through the determination of scaling laws, which can be used to characterize and predict the fundamental properties of a system requiring only the knowledge of simple input parameters.

Previous studies have investigated, for example, the scaling of density and granular temperature fields in one [11], two [12], and three dimensions [13]. Numerous studies have also focused on the scaling behaviours of a granular bed's vertical center of mass, h, which can be used as a measure of the potential energy of a granulate. For granular systems within which the distribution of granular temperature T can be considered approximately uniform, changes in the system's center of mass from its resting value are also proportional to T [14], making an understanding of the behavior of h very valuable. Theoretical and simulational work by Luding *et al.* demonstrated that, both in one-dimensional [15] and two-dimensional [16] systems, the center of mass of a granulate scales approximately as:

$$h = h_0 + \frac{C(A_0\omega)^{\alpha}}{[N_l(1-\varepsilon)]^{\beta}}, \tag{1}$$

where h_0 is the center of mass of a system at rest, A_0 and $\omega = 2\pi f$ are, respectively, the amplitude and frequency with which the system is driven, $N_l = \frac{Nd^2}{L_x L_y}$ is proportional to the number of particle layers in the system (with d the particle diameter and $L_{x,y}$ the system's horizontal dimensions), ε is the particles' coefficient of restitution and C is a constant. The exponent α was found to be equal to 2 in one dimension and 3/2 in two dimensions. The two-dimensional scaling of h was subsequently investigated by Warr *et al.* [17], who found the scaling to be applicable also to experimental systems, albeit with differing exponents; specifically, they found their system to scale approximately as $C(A_0\omega)^{1.3}[N_l(1-\varepsilon)]^{-0.3}$. This departure from the scaling of Ref. [16] was attributed largely to the presence of additional forces due to particle-wall interactions not accounted for in the original simulational work. Experimental NMR studies by Yang and Candela [18] showed the scaling of Luding *et al.* to hold even in three dimensions, this time with $\alpha = 1.0 \pm 0.2$. They also found the center of mass to scale with the bed height as $h - h_o \propto N_l^{0.5}$.

Although the general scaling relationship discussed above has been shown to be relevant to one-, two-, and three-dimensional granulates, until now the theory has only been tested in *monodisperse* systems. Granular materials in industrial and other real-world scenarios, however, are often composed of two or more different species of particle, and may exhibit complex behaviors not observed in the single-species case. The aim of this current study is to relax the constraint of monodispersity by demonstrating that scaling similar to that of Refs. [15,16] can be extended to bidisperse systems. Through investigation of binary systems of equally sized particles differing in their material densities, we modify equation (1) to account for mass differences between particle species, as well as the effects of density-driven segregation [19,20]. Through a combination of simulation and experiment, we verify the modified scaling for a range of ω, A_0, and N_l.

II. EXPERIMENTAL DETAILS

A. System details

The experimental system comprises a square-based cuboid container of width $L_x = L_y = 80$ mm and height $L_z = 200$ mm, within which is housed a bed of $2400 \leqslant N \leqslant 6700$ spherical particles of diameter $d = 3$ mm, corresponding to a range of dimensionless resting bed heights $3.4 \leqslant N_l \leqslant 9.4$. The height of the container is adequate to minimize the probability of particle collisions with the system's upper boundary, meaning that the system can be considered effectively open, while the dimensionless width of the container, $\widetilde{L}_{x,y} = L_{x,y}/d = 26.7$ ensures that the system can be considered fully three dimensional. The relatively large size of the particles used allows interstitial air effects to be neglected [21], and the possible influence of static electricity in the system is reduced through the use of a conductive steel base plate [22]. The container is affixed to an LDS V721 electrodynamic shaker,

TABLE I. Effective elasticities, ε_{AA}, and material densities, ρ, for the various particles used in experiment.

Particle Material	ρ (kgm^{-3})	ε_{AA}
Nylon (N)	1134	0.41
Glass (G)	2500	0.83
Steel (S)	7850	0.79
Brass (B)	8500	0.61

and subjected to sinusoidal vibrations in the vertical direction. The system is vibrated at a fixed frequency $f = 40$ Hz with a range of amplitudes $A_0 \in (0.388, 1.71)$ mm, corresponding to a range of dimensionless accelerations $\Gamma = \frac{4\pi^2 f^2 A_0}{g}$ between 2.5 and 11. The use of a fixed dimensionless frequency $\bar{\omega} = 2\pi f\sqrt{d/g} > 1$ ensures that the bed maintains a fluidized state for all data sets [18,23].

Particles of various materials, and hence material densities, ρ, are used in experiment; specific details can be seen in Table I. Alongside each material's density, the table also gives values of effective elasticity for interparticle collisions between similar grains, ε_{AA}. Effective elasticity is a measure of the average energy lost by a particle during a collision, determined experimentally by taking the mean value of energy loss over a large number of collisions in a single-component system [24]. Several combinations of particle species are investigated, providing a range of binary systems with a variety density ratios. For each combination, equal numbers of each species are used, i.e., $N_A = N_B = N/2$. 0.5 g of graphite powder is added to each experimental system to act as a lubricant, minimizing the influence of frictional interactions [25]. This suppression of frictional forces allows effects due to elasticity to be isolated, simplifying analysis and enabling more reliable comparison with both theory and simulation.

B. Data acquisition: Positron emission particle tracking

Experimental data is acquired using positron emission particle tracking (PEPT), a noninvasive technique capable of imaging a granular system in three dimensions with millimeter spatial resolution and temporal resolution of the order of milliseconds [26]. PEPT uses a dual-headed γ camera to track the three-dimensional motion of a single tracer particle, which has been labeled with a β^+-emitting radioisotope. The back-to-back γ rays emanating from the tracer particle can be used to rapidly triangulate its spatial position and hence record its motion through a system. Aside from being radioactively labeled, the tracers used in our experiments are physically identical to the other particles in the bed.

For systems in a steady state, and for experiments of adequate duration, the time-averaged behavior of a single tracer particle can, due to the principle of ergodicity, be considered representative of the spatially averaged behaviors of all similar particles in the system. In the case of binary systems, one need simply conduct two identical runs, one with a tracer of species A and one with a tracer of species B; information from these two runs can then be combined to give information pertaining to the entire system. PEPT can be used to extract various important quantities from a granular system including, but not limited to, density, velocity and temperature fields [27,28], mean-squared displacements and diffusion coefficients [29], convection strengths [30,31] and, for binary and polydisperse systems, particle concentration distributions and segregation intensities [32]. The ability of PEPT to probe the interior of large, dense, and/or opaque three-dimensional systems is particularly useful as it facilitates the analysis of particle distribution in three dimensions, meaning that segregation can be accurately characterized even for wide systems with high packing fractions, a feat that is difficult to achieve with other experimental methods.

Data for each experimental system is acquired over a period of between 3600 and 7200 s, dependent on the values of Γ and N_l for a given system—particles within deeper or less strongly vibrated systems will naturally be less mobile, meaning that it will take longer for the tracer to explore the entire system and hence gain adequate statistics. In all instances, it is ensured that the system has reached its equilibrium distribution and is in a steady state: each 3600–7200 s data set is separated into a series of 200 s segments and the particle distributions for each segment measured, ensuring that they remain consistent for the duration of the run.

C. Determination of relevant quantities

1. *Packing fractions and particle distributions*

As discussed in the previous section, due to the ergodicity of the steady-state systems under investigation, the time-averaged behavior of a single particle may be considered equivalent to an ensemble average for a large system of particles. Thus, the residence time fraction, F, of a particle in a given region of the system can be assumed proportional to the local packing fraction within this region. In order to calculate a one-dimensional packing profile in the vertical (z) direction, one need simply consider a series of horizontal slices through the experimental system, each of volume V_s. With knowledge of the relative fraction of time spent by the tracer in each of these segments, the height-dependent packing fraction, $\eta(z)$, can be determined as:

$$\eta(z) = \frac{\pi d^3 N F(z)}{6V_s}. \tag{2}$$

For bidisperse and polydisperse systems, a similar treatment can be applied to both/all species allowing, in addition to the bulk packing profiles, the distributions and local concentrations of particles to be determined. Examples can be seen in Fig. 2, demonstrating the excellent agreement between experimentally determined and simulated particle distributions.

2. *Segregation intensity*

The degree to which a system exhibits segregation can be quantified by a segregation intensity I_s analogous to that defined in Ref. [33]. Although it is possible to calculate the intensity of segregation in all three spatial dimensions, for the purposes of the current study we need only consider segregation in the vertical direction. For this case, I_s can be determined by dividing the system into a series of N_s equally sized horizontal segments. The local number fraction or concentration of a single species for the ith segment is denoted

φ_i^A; in the case of a binary system, $\varphi^A = \eta^A/(\eta^A + \eta^B)$ where the superscripts A and B denote particle species. By determining the local concentration for all N_s segments, I_s can be calculated as:

$$I_s = \left[\frac{\sum_{i=1}^{i=N_s}\left(\varphi_i^A - \varphi_m\right)^2}{N_s}\right]^{\frac{1}{2}}, \qquad (3)$$

where φ_m is the system's mean concentration. A value $I_s = 0$ represents a perfectly mixed system. while the maximal value of I_s for a given system is indicative of complete segregation.

III. SIMULATIONS

Discrete particle simulations are conducted using the MERCURYDPM code [34–37] developed at the University of Twente. Values of f, A, N_l, d, ρ, and ε_{AA} are taken as the experimental values given above. The frictional coefficient μ is set to 0 in order to reproduce the suppression of friction in the experimental system due to the use of graphite lubricant. For interspecies collisions, the effective elasticity ε_{AB} is taken as the geometric average of the relevant single-species values. This determination of ε_{AB} arises as a natural consequence of the spring-dashpot model of particle restitution [38–40] and, despite its simplicity, demonstrates strong agreement with experimental data in all cases. The simulations implement inelastic, vertical sidewalls with coefficient of restitution $\varepsilon_w = 0.59$, equal to the experimentally measured value for a particle-wall collision involving a glass particle. Although the value of ε_w is likely to vary slightly depending on the dissipative properties of the particles involved, the precise value was found not to significantly affect the sytem's behavior as long as it remained sufficient to ensure the suppression of buoyancy-driven convective motion [31,41].

IV. RESULTS AND ANALYSIS

A. Variation of center of mass with density ratio

Figure 1 demonstrates how the alteration of the relative particle masses in a binary granular bed can significantly affect the position of the system's center of mass, h, even when all other parameters are held constant. The explanation for this behavior is simple: as the ratio ρ_H/ρ_L diverges from unity, the system becomes increasingly segregated [22]. Buoyancy effects within the fluidized system [42], will cause heavier particles to preferentially sink to the bottom of the container and, conversely, lighter particles to rise toward the free surface. The larger the density ratio, the more complete the separation of the two species. Clearly, this increase in segregation, combined with an increased disparity between particle masses, will result in a decreased center of mass for the system. An illustrative example of the variation in segregation intensity, and hence center of mass position, with ρ_H/ρ_L can be seen in Fig. 2. It is worth noting the strong agreement between simulations and experimental results demonstrated in Figs. 1 and 2.

For the equal-elasticity simulations shown in Fig. 1, the various combinations of ρ_H and ρ_L used to create the range of the density ratios shown are chosen such that $\rho_{\text{ave}} = \frac{1}{2}(\rho_H + \rho_L)$ is equal to 5000 kgm^{-3} in all instances. Indeed,

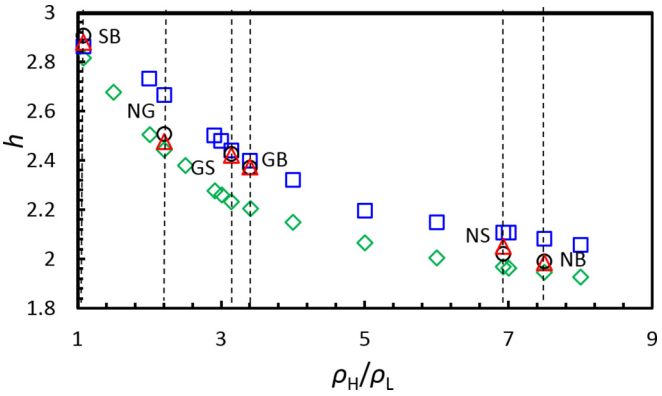

FIG. 1. (Color online) Variation of vertical center of mass position with density ratio ρ_H/ρ_L for systems of resting height $N_l = 5.4$ driven with acceleration $\Gamma = 3.5$. Data is shown for experiment (black circles) and the corresponding simulations (red triangles), which implement the experimental values of the relevant parameters. Data is also shown for simulations in which only density differences between particles are considered, i.e., $\varepsilon_{AA} = \varepsilon_{BB}$; blue squares and green diamonds correspond to the cases $\varepsilon_{AA} = \varepsilon_{BB} = 0.83$ and $\varepsilon_{AA} = \varepsilon_{BB} = 0.41$ respectively. The letters given in the figure denote the combination of particle materials used in experimental measurements, as given in Table I.

unless stated otherwise, this is the case for all data presented in this manuscript. The decision to hold ρ_{ave} constant was taken to ensure consistency, the specific value of 5000 kgm^{-3} being chosen due to the fact that it is approximately equal to the average density of all particle materials used in experiment. However, due to the nature of the systems under investigation,

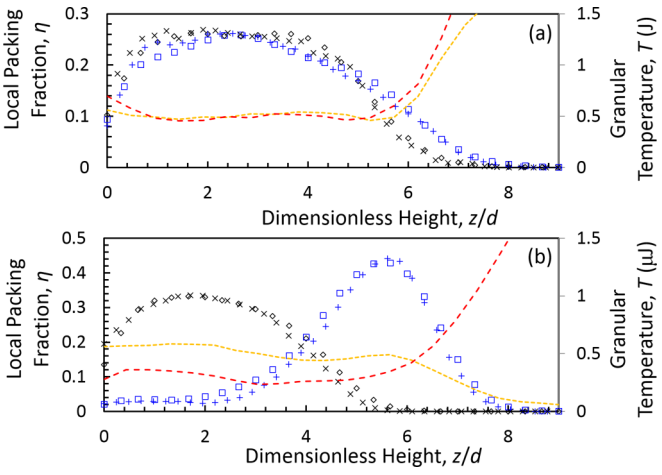

FIG. 2. (Color online) Spatially averaged one-dimensional packing and temperature profiles for the case $\Gamma = 6.5$, $N_l = 5.4$ with (a) $\rho_H/\rho_L = 1.08$ (steel and brass particles) and (b) $\rho_H/\rho_L = 7.50$ (nylon and brass particles). h_L, h_H, and h denote, respectively, the center of mass positions of the light component of the system, the heavy component of the system and the bed as a whole. In each panel, the light and heavy components are represented, respectively, by squares and diamonds for the simulated data and by upright and diagonal crosses for experimental data. Temperature profiles extracted from simulated data are shown, in each case, for both the light (red dashed line) and heavy (orange dotted line) particle species.

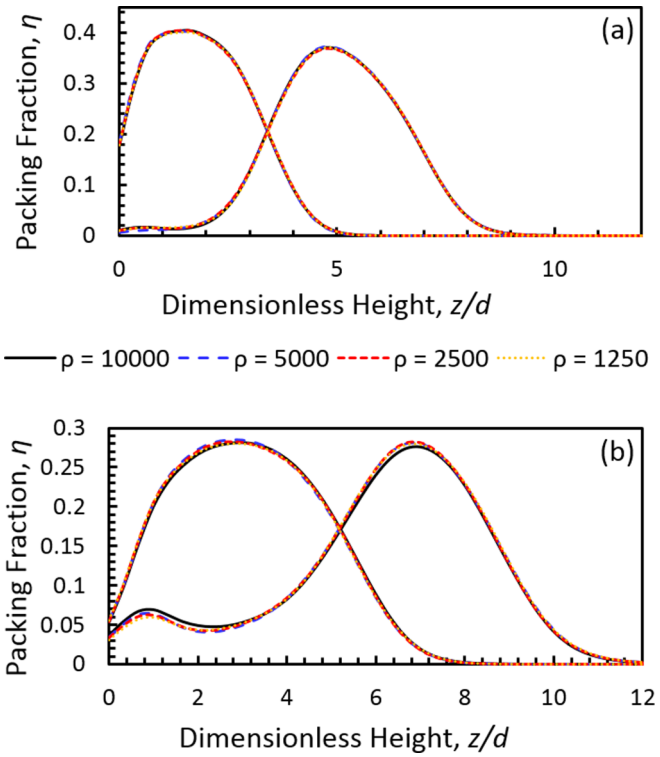

FIG. 3. (Color online) One-dimensional packing profiles for bidisperse beds with $N_l = 5.4$, $\varepsilon_{AA} = \varepsilon_{BB} = 0.83$ and $\rho_H/\rho_L = 4$ driven with dimensionless accelerations (a) $\Gamma = 3.5$ and (b) $\Gamma = 11$. For each value of Γ, the fixed density ratio of 4 is achieved using different combinations of particle masses, resulting in particles' average material densities ranging from 1250 kgm^{-3} to 10000 kgm^{-3}.

the results discussed here may in fact be generalized to similar systems of arbitrary average density; Fig. 3 shows systems for which the density *ratio* is held constant while the *average* density of the system is varied. The image clearly shows the center of mass of the systems to be effectively mass invariant over the range of average densities shown, which were deliberately chosen to exceed both the maximal and minimal values explored in experiment. This decoupling of the system's average density (or, equivalently, total mass) from the center of mass height may be expected for the case of simulations in which particles are driven by an infinitely heavy wall. In some experimental situations, though, this decoupling may prove less strict due to, for instance, an increased mass of particles interfering with the driving of the system. This is not an issue in the experiments presented here, however, due to our use of feedback from an accelerometer to ensure consistency in the base motion for all systems.

It is clear from Fig. 1 that particle elasticity, and differences therein between particle species, may cause deviation from the relatively smooth trend observed for the case in which only density is varied. Particle elasticity can be expected to influence a system's center of mass in two ways: first, by creating a more compacted bed which, clearly, will lower the system's center of mass, and secondly through an alteration in the system's segregative behaviors [43–46]. The influence of inelasticity in our system is elucidated through the inclusion of two simulated data sets for which $\varepsilon_{AA} = \varepsilon_{BB}$. The first series of simulations sets the elasticity value to 0.83, the maximal value used in experiment, while the second implements the minimal value, $\varepsilon = 0.41$. These two curves thus represent the absolute upper and lower boundaries between which all data points may be expected to lie. Hence, for cases in which the system's average elasticity is close to that of the highly elastic glass particles (e.g., for the GS system, where $\varepsilon_{\mathrm{ave}} = 0.81$), experimental data points lie close to the upper curve. Conversely, for particularly dissipative systems (such as the NB system for which $\varepsilon_{\mathrm{ave}} = 0.51$), experimental results approach instead the lower limit. Since the primary focus of the current study is the case of density-driven segregation, simulations will, unless otherwise stated, be conducted using equal particle elasticities, such that any trends relating to density differences will not be obscured by the competing segregative mechanisms arising from inelasticity differences. Nonetheless, comparisons with experimental results will still include accurate values of inelasticity, as is the case in Figs. 1 and 2.

In addition to the variation with z of the system's local solids fraction, Fig. 2 also shows one-dimensional vertical T profiles corresponding to the partial temperatures of the differing system components. It is notable in Fig. 2(b), where a significant difference exists between particle masses, there exists also a considerable disparity between the temperatures of the different particle species. This violation of the principle of energy equipartition may be expected from the findings of previous studies [24,28]. The approximately constant ratio of the individual components' temperatures throughout the bulk of the system also agrees with the existing literature [24,43]. We also observe, once again in agreement with previous works [47], that the observed difference between species' typical temperatures becomes more pronounced with an increasing disparity in density. Crucially, however, for all instances discussed in this paper, both components of the temperature (and hence, clearly, the total temperature) remain approximately constant across the bulk of the system, exhibiting significant gradients only in the dilute region near the system's free surface and in close proximity to the systems energy source at the lower boundary.

It has been shown, for dilute systems in the tracer limit [43,44] and, subsequently, for more general gaseous systems [48] that temperature differences between particle species may significantly affect the segregative behaviours of granulates due to the presence of thermal diffusion. However, for less dilute systems and in the absence of significant temperature gradients, as is the case here, segregation is most likely to be driven predominantly by buoyancy forces [49,50]. Regardless of the specific mechanism by which segregation occurs in the current system, as long as the resultant I_s value is known, the observed temperature differences do not seem to have any effect on the system's center of mass significant enough to cause substantial deviation from our scaling predictions. Although beyond the scope of the current study, the authors hope that future work may be able to combine the findings of this paper with those of Refs. [43–50] to produce a generalized and truly predictive model capable of prognosticating both the degree of segregation and center of mass position of a system based only on simple input parameters.

B. Modification of the scaling relationship

Having established the existence of a relationship connecting a system's center of mass position, h, to the density ratio between particle species, ρ_H/ρ_L, and the degree of segregation within the system, I_s, we now attempt to modify the scaling law of Ref. [16] to account for these extra parameters. Of course, we must also consider the effect of extending the system into the third dimension. Experimental and simulational analyses of monodisperse systems suggest, for a our current setup, scaling exponents $\alpha = 1$ and $\beta = 1$. Specifically, the best linear fit for a log-log plot of $h - h_0$ against $A_0\omega$ gives a gradient, and hence an α value, of 0.92 ± 0.10; however, a value of 1.0 is also found to show acceptable agreement. Thus, for the sake of simplicity, we assume $h - h_0 \propto A_0\omega$. The line of best fit for a logarithmic plot of $h - h_0$ as a function of $N_l(1-e)/A_0\omega$, meanwhile, gives a slope of 1.04 ± 0.06, strongly indicating a $\beta = 1$ scaling.

The obtained value of α not only makes sense phenomenologically through its continuation of the trend of decreasing α with increasing dimensionality, but also shows reasonable agreement with the exponent previously determined for a three-dimensional system by Yang and Candela [18]. The value of β agrees well with the original scaling of Luding *et al.* in both one and two dimensions, yet differs significantly from that determined in Ref. [18]. There are two likely causes of this considerable disparity. First, the experimental system used in the current study is considerably larger than that used in Ref. [18], with dimensionless width $\widetilde{L} \approx 26.7$ as opposed to $\widetilde{L} \approx 4.4$ for the earlier work. The increased system size of the current setup will result in a considerably decreased influence of particle-wall interactions compared to the previous study; wall effects have previously been shown to affect scaling behavior through the introduction of additional frictional forces not accounted for by the original theory [17]. Similarly, the addition of graphite lubricant to our experimental system will also result in a reduced importance of frictional effects compared to previous experimental studies.

We now turn our attention to the effects of the density ratio and segregation intensity. We begin by considering the extremal cases of perfect mixing and complete segregation, ignoring for the time being bed expansion due to other processes. In the former case, the centers of mass for both particle species will be $0.5z_{\max}$, $z_{\max}$ being the height of the system. In the latter case, the centers of mass for the light and heavy species will be, respectively, at their maximum and minimum values, i.e., $h_L = h_L^{\max}$ and $h_H = h_H^{\min}$. The values of $h_L^{\max}$ and $h_H^{\min}$ can, for a given system, be easily determined from the relative number of each species, e.g., for a 50 : 50 mixture, $h_L^{\max} = 0.75N_l$ and $h_H^{\min} = 0.25N_l$. Clearly, the values of h_L and h_H are dependent upon the segregation intensity, I_s, within the system. For a perfectly mixed system, $I_s = 0$, with its maximal value, $I_s^{\max}$, being achieved in a fully separated system. For binary systems in which $N_H = N_L$ (as is the case for the main results discussed within this paper), $I_s^{\max} = 0.5$. However, for systems of varying composition, this value will differ. Thus, to ensure generality, throughout this manuscript we will refer simply to $I_s^{\max}$, without assigning to this quantity a specific numerical value. If we assume that the positions of the centers of mass for the heavy and light components vary linearly with I_s, we can write that:

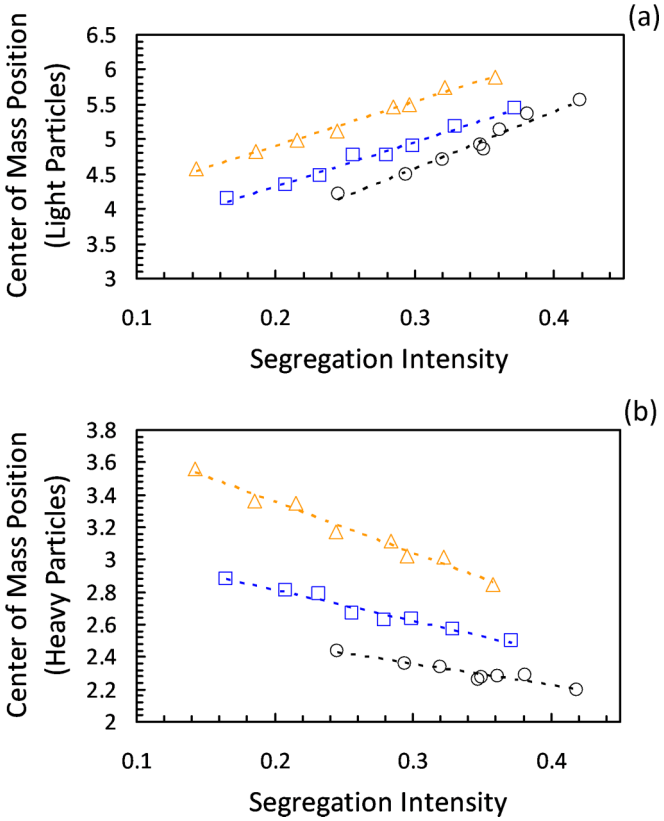

FIG. 4. (Color online) Variation of h_L and h_H with segregation intensity. Data is shown for simulations with resting bed height $N_l = 5.4$ driven with accelerations $\Gamma = 6.5$ (circles), $\Gamma = 8$ (squares) and $\Gamma = 9.5$ (triangles). In each case, the degree of segregation is altered through variation of the relative masses of the two particle species whilst keeping all other parameters, including the total mass, M, of the system, constant.

$$h_L = z_{\max}\left[0.5 + \left(\frac{I_s}{I_s^{\max}}\Delta h_L^{\max}\right)\right] \tag{4}$$

and

$$h_H = z_{\max}\left[0.5 - \left(\frac{I_s}{I_s^{\max}}\Delta h_H^{\min}\right)\right], \tag{5}$$

where $\Delta h_L^{\max}$ is the magnitude of the difference in center of mass position of light (L) particles between the fully segregated and fully mixed cases, i.e., $\Delta h_L^{\max} = |h_L^{\max} - h_L^{I_s=0}|$. Similarly, for the heavier (H) species, $\Delta h_H^{\min} = |h_H^{\min} - h_H^{I_s=0}|$. Despite its simplicity, the assumption of a linear relationship between species' centers of mass and I_s is well supported by the data, as exemplified in Fig. 4. Using the calculated centers of mass, it is then possible to modify the h_0 term of Eq. (1) to account for the variation of ρ_H/ρ_L and I_s:

$$h_0^* = \frac{h_L M_L + h_H M_H}{M_L + M_H} \tag{6}$$

where M_L and M_H are the total masses of light and heavy particles respectively.

The end result of our modification to the scaling law of Luding *et al.* is, in essence, to account for the shift in the

system's center of mass due to the uneven distribution of dissimilarly massive particles, which acts in addition to the center of mass change due to the bed's expansion accounted for by the original scaling. For the case in which the system exhibits no segregation, or for which particles are equally massive, the scaling reduces to the same basic form of the original with $h_0^* = h_0 = 0.5 z_{\max}$, as would be expected.

It is worth noting that h_0 is no longer necessarily the true resting center of mass of the system—clearly, a bidisperse granular system at rest could be arranged to give an arbitrary number of different centers of mass; rather, the modified h_0 is the center of mass position for a bed at rest yet possessing the I_s value of the relevant excited state.

C. Comparison with simulation and experiment

Figure 5 compares experimental and simulated data to both the modified and unmodified scaling relations [Eq. (1)]. In order to isolate the effects of density and segregation intensity, the elasticity coefficients of both species are held constant at a value of $\varepsilon_{AA} = \varepsilon_{BB} = 0.8$. For experimental data sets, the ε term in Eq. (1) is taken as the geometric average of ε_{AA} and ε_{BB}. In all instances, the scaling exponents are taken as $\alpha = 1$ and $\beta = 1$. The considerably improved agreement for the modified scaling clearly demonstrates the importance of considering the effects of ρ_H/ρ_L and I_s. Figure 6 compares theoretical and simulational results for various combinations of Γ and N_l, showing the theory to be robust over a considerable range of system parameters. Specifically, simulation and theory were found to show reasonable agreement over the entire range of driving strengths ($2.5 \leqslant \Gamma \leqslant 11, 0.1 \leqslant A_0\omega \leqslant 0.43$ ms^{-1}), bed heights ($3.4 \leqslant N_l \leqslant 9.4$) and density ratios ($1 \leqslant \rho_H/\rho_L \leqslant 15$) tested. The scaling was, however, found to break down for specific combinations of Γ and N_l producing systems with particularly high densities and collision rates, resulting in a situation for which the assumption $t_{ev}/t_c \gg 1$ of the original theory [16] is no longer valid. Here, t_{ev} is the average time between collision events and t_c is the typical duration of particle collisions. The scaling behavior was also found to hold across the tested range of particle concentrations, $\phi_m \in (\frac{1}{4}, \frac{3}{4})$.

Although for the main results presented frictional effects are minimized, the effect of friction was tested using both unlubricated experimental beds and simulations with nonzero μ values, in order to test the applicability of the theoretical scaling to more highly frictional systems. In simulation, a variety of systems with frictional coefficients $\mu = 0.1, 0.5$, and 1.0 were investigated; in experiment, comparison was drawn between various identical systems both with and

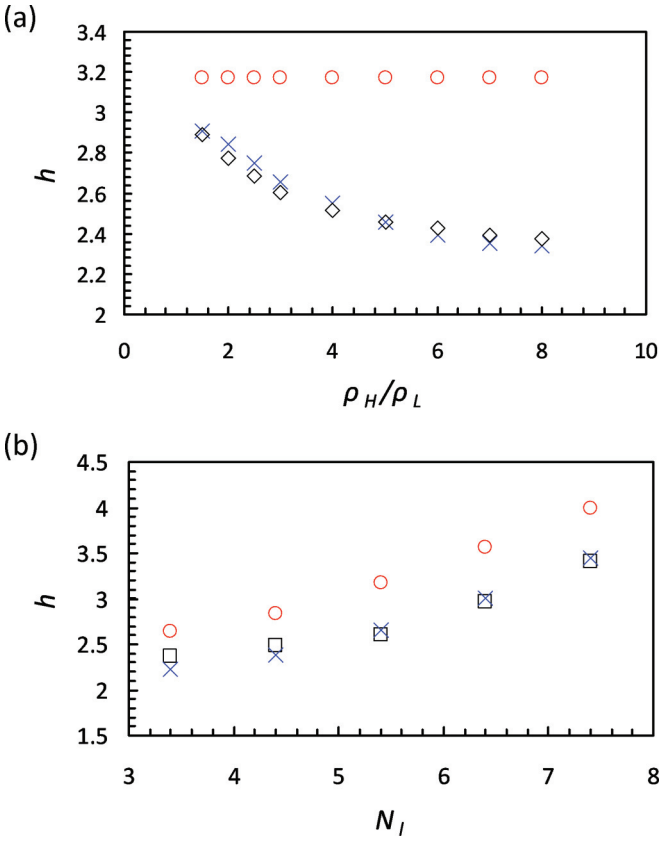

FIG. 5. (Color online) (a) Variation of a binary system's center of mass, h, with the density ratio between particle species, ρ_H/ρ_L, for the case of $\Gamma = 5$, $N_l = 5.4$ and equal numbers of each particle species, $N_L = N_H$. Diamonds represent data acquired from simulations. Shown also is the theoretical scaling according to Eq. (1) for the case in which density and segregation effects are considered (crosses) and the case in which they are neglected (circles). (b) Experimental results (squares) for fixed $\rho_H/\rho_L = 3.14$ corresponding to a system of glass and steel spheres. Here, Γ is held at a constant value of 5, while N_L is varied. Once again, theoretical scaling according to the modified and unmodified versions of Eq. (1) are represented by crosses and circles respectively. In all cases, the scaling exponents α and β are set equal to unity, as discussed in the text.

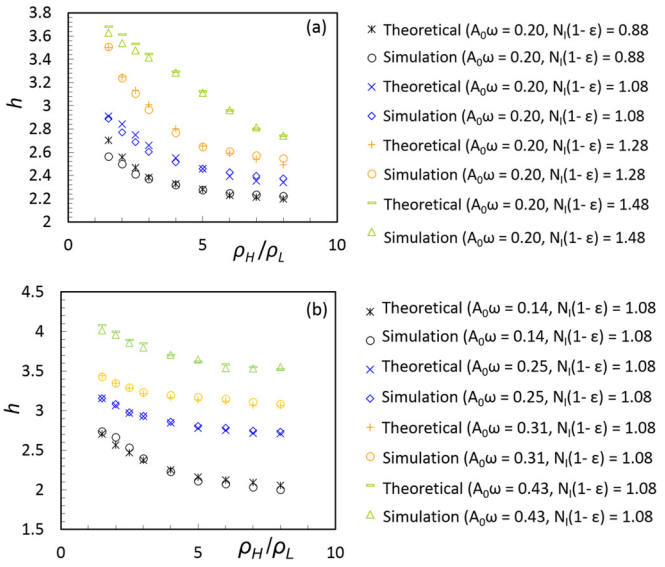

FIG. 6. (Color online) Comparison of simulational and theoretical results showing the variation of h with ρ_H/ρ_L for (a) a variety of Γ values at fixed $N_l = 5.4$ and (b) a variety of N_l values at fixed $\Gamma = 5$. As with Fig. 5, the scaling predictions are determined using exponents $\alpha = \beta = 1$. The agreement shown between simulational results and scaling predictions across a range of $A_0\omega$ and $N_l(1-\varepsilon)$ values provides strong support for the idea that the model of Luding *et al.* may indeed be successfully extended to the bidisperse case.

without lubricant. The results showed that in the fluidized systems considered, friction acts simply as an additional source of energy loss. Thus, since an increase in friction can be considered equivalent to a decrease in the relevant effective elasticity values, frictional effects may be accounted for through a simple alteration in the ε value used in the scaling; indeed in experiment, these effects are already accounted for during the determination of particles' effective elasticities. It is also perhaps worth noting that, in experiment, the differences between the lubricated and unlubricated system were, in general, found to be small.

Additional tests conducted outside of the parameter range of the main experiment, using Γ values of up to 25 ($A_0\omega = 0.66$ ms^{-1}) and bed heights of up to 15, strongly imply that the scaling may be expected to hold for *any* system for which $t_{ev}/t_c \gg 1$ and T may be assumed approximately uniform throughout the bulk of the bed.

It should be noted that although the scaling law presented holds across a significant range of parameter space, it remains reliant on a lack of significant density and temperature gradients or convective motion, as well as the condition of fluidization, thus limiting its generality. Nonetheless, the strong agreement observed for systems obeying these constraints provides support for the possibility that theories developed for monodisperse granular systems may successfully extended to the binary case, a matter with potentially important implications in the field of granular dynamics.

V. SUMMARY AND CONCLUSION

We have shown that the center of mass scaling relation first determined by Luding *et al.* [15,16] for monodisperse one- and two-dimensional granular beds may, through simple modifications, be successfully applied to fully three-dimensional, binary granular systems. Close quantitative agreement of the theoretical scaling with both experimental data acquired using positron emission particle tracking and simulations produced using the MERCURYDPM code [37] strongly implies the relation to be valid over a considerable range of system parameters. Although the current scaling relation only applies to systems, which are bidisperse by density, through further modification it should be possible to account also for differences in particle size and elasticity, or indeed other relevant parameters. Thus, we hope that this work may form an incremental step towards the eventual formation of a scaling law applicable even to complex industrial systems and other important, real-world applications.

ACKNOWLEDGMENTS

The authors would like to thank Mr. Nicolás Rivas, Dr. Thomas Weinhart, and Professor Anthony Thornton for fruitful discussions and Professor Stefan Luding for both his valuable input as well as access to the computer facilities on which the simulations in this paper were performed. We gratefully acknowledge the financial support of the Hawkesworth Scholarship, kindly provided by the late Dr. Michael Hawkesworth.

[1] R. L. Brown, J. Inst. Fuel **13**, 15 (1939).
[2] K. M. Aoki, T. Akiyama, Y. Maki, and T. Watanabe, Phys. Rev. E **54**, 874 (1996).
[3] F. Melo, P. Umbanhowar, and H. L. Swinney, Phys. Rev. Lett. **72**, 172 (1994).
[4] K. Ahmad and I. J. Smalley, Powder Technol. **8**, 69 (1973).
[5] A. Rosato, K. J. Strandburg, F. Prinz, and R. H. Swendsen, Phys. Rev. Lett. **58**, 1038 (1987).
[6] A. D. Rosato, D. L. Blackmore, N. Zhang, and Y. Lan, Chem. Eng. Sci. **57**, 265 (2002).
[7] H. M. Jaeger, S. R. Nagel, and R. P. Behringer, Rev. Mod. Phys. **68**, 1259 (1996).
[8] S. S. Hsiau, C. C. Liao, P. Y. Sheng, and S. C. Tai, Exp. Fluids **51**, 795 (2011).
[9] D. U. Ringer and A. S. Mujumdar, Drying Technol. **2**, 449 (1983).
[10] S. Satija and I. L. Zucker, Drying Technol. **4**, 19 (1986).
[11] S. Warr and J. M. Huntley, Phys. Rev. E **52**, 5596 (1995).
[12] J. Lee, Physica (Amsterdam) **219D**, 305 (1995).
[13] V. Kumaran, Phys. Rev. E **57**, 5660 (1998).
[14] J. M. Huntley, Phys. Rev. E **58**, 5168 (1998).
[15] S. Luding, E. Clément, A. Blumen, J. Rajchenbach, and J. Duran, Phys. Rev. E **49**, 1634 (1994).
[16] S. Luding, H. J. Herrmann, and A. Blumen, Phys. Rev. E **50**, 3100 (1994).
[17] S. Warr, J. M. Huntley, and G. T. H. Jacques, Phys. Rev. E **52**, 5583 (1995).
[18] X. Yang and D. Candela, Phys. Rev. Lett. **85**, 298 (2000).
[19] D. C. Hong, P. V. Quinn, and S. Luding, Phys. Rev. Lett. **86**, 3423 (2001).
[20] D. A. Huerta and J. C. Ruiz-Suárez, Phys. Rev. Lett. **92**, 114301 (2004).
[21] C. Zeilstra, M. A. van der Hoef, and J. A. M. Kuipers, Phys. Rev. E **77**, 031309 (2008).
[22] Q. Shi, G. Sun, M. Hou, and K. Lu, Phys. Rev. E **75**, 061302 (2007).
[23] P. Sunthar and V. Kumaran, Phys. Rev. E **64**, 041303 (2001).
[24] K. Feitosa and N. Menon, Phys. Rev. Lett. **88**, 198301 (2002).
[25] J. S. van Zon, J. Kreft, D. I. Goldman, D. Miracle, J. B. Swift, and H. L. Swinney, Phys. Rev. E **70**, 040301 (2004).
[26] D. J. Parker, R. N. Forster, P. Fowles, and P. S. Takhar, Nucl. Instrum. Methods Phys. Res., Sect. A **477**, 540 (2002).
[27] R. D. Wildman, J. M. Huntley, and D. J. Parker, Phys. Rev. E **63**, 061311 (2001).
[28] R. D. Wildman and D. J. Parker, Phys. Rev. Lett. **88**, 064301 (2002).
[29] R. D. Wildman, J. M. Huntley, J.-P. Hansen, D. J. Parker, and D. A. Allen, Phys. Rev. E **62**, 3826 (2000).
[30] R. D. Wildman, J. M. Huntley, and D. J. Parker, Phys. Rev. Lett. **86**, 3304 (2001).
[31] C. R. K. Windows-Yule, N. Rivas, and D. J. Parker, Phys. Rev. Lett. **111**, 038001 (2013).
[32] C. R. K. Windows-Yule, T. Weinhart, D. J. Parker, and A. R. Thornton, Phys. Rev. Lett. **112**, 098001 (2014).
[33] D. V. Khakhar, J. J. McCarthy, T. Shinbrot, and J. M. Ottino, Phys. Fluids **9**, 31 (1997).

[34] A. R. Thornton, D. Krijgsman, A. te Voortwis, V. Ogarko, S. Luding, R. Fransen, S. Gonzalez, O. Bokhove, O. Imole, and T. Weinhart, *DEM 6: 6th International Conference on Discrete Element Methods and Related Techniques* (Colorado School of Mines, Colorado, 2013), p. 393.
[35] A. R. Thornton, T. Weinhart, S. Luding, and O. Bokhove, Int. J. Mod. Phys. C **23**, 1240014 (2012).
[36] A. R. Thornton, T. Weinhart, V. Ogarko, and S. Luding, Comput. Meth. Mat. Sci. **13**, 197 (2013).
[37] www.MercuryDPM.org
[38] P. A. Cundall and O. D. L. Strack, Geotechnique **29**, 47 (1979).
[39] S. Luding, Granular Matter **10**, 235 (2008).
[40] T. Weinhart, A. R. Thornton, S. Luding, and O. Bokhove, Granular Matter **14**, 531 (2012).
[41] J. Talbot and P. Viot, Phys. Rev. Lett. **89**, 064301 (2002).
[42] N. Shishodia and C. R. Wassgren, Phys. Rev. Lett. **87**, 084302 (2001).
[43] J. J. Brey, M. J. Ruiz-Montero, and F. Moreno, Phys. Rev. Lett. **95**, 098001 (2005).
[44] J. J. Brey, M. J. Ruiz-Montero, and F. Moreno, Phys. Rev. E **73**, 031301 (2006).
[45] R. Brito, H. Enriquez, S. Godoy, and R. Soto, Phys. Rev. E **77**, 061301 (2008).
[46] R. Brito and R. Soto, Eur. Phys. J. Spec. Top. **179**, 207 (2009).
[47] J. J. Brey and M. J. Ruiz-Montero, Phys. Rev. E **84**, 031302 (2011).
[48] V. Garzó, Europhys. Lett. **75**, 521 (2006).
[49] L. Trujillo and H. J. Herrmann, Granular Matter **5**, 85 (2003).
[50] L. Trujillo, M. Alam, and H. J. Herrmann, Europhys. Lett. **64**, 190 (2003).